Global NEST Journal, **28** (6), 08079
Available online: 02/07/2026

Design and Characterization of LDH-Modified Biochar as a Nanoadsorbent for Copper Removal: A Response Surface Methodology Approach

M. Shafiq[a, *], M. T. Amin[b], A. A. Alazba[a, c]

[a]Water Research Chair, King Saud University, Riyadh 11451, Saudi Arabia.
[b]Civil and Environmental Engineering Department, College of Engineering, King Faisal University, Al-Ahsa 31982, Saudi Arabia
[c]Department of Agricultural Engineering, College of Food and Agricultural Sciences, King Saud University, Riyadh 11451, Saudi Arabia.

*Correspondence e-mail: msrana@ksu.edu.sa

Abstract

This study reports the layered double hydroxides' modified wheat straw biochar (WsBio-LDH composite) composite as an effective adsorbent for the removal of copper ions (Cu^{2+}) from aqueous solution. The WsBio-LDH composite adsorbent was analyzed using central composite design and response surface methodology (RSM). RSM optimized parameters for Cu^{2+} removal using the WsBio-LDH composite were found to be 87.06 min for the contact time, 0.491 g for the adsorbent dose, 5.93 for the solution pH, and 12.75 mg/L for the initial Cu^{2+} concentration. A significant correlation between predicted and experimental values was observed with 99 % removal exhibiting a deviation of less than 1% that validates the model's accuracy. All individual batch variables significantly ($p<0.0001$) influenced the Cu^{2+} removal efficiency using the WsBio-LDH composite. Both the contact time and initial Cu^{2+} concentrations displayed negative effects while the solution pH and Cu^{2+} concentrations exerted a positive interactive effect ($p <0.0049$) on Cu^{2+} removal efficiency using the WsBio-LDH composite. The Langmuir model accurately represented a monolayer adsorption of Cu^{2+} onto the surface of the WsBio-LDH composite. The pseudo-second order kinetic model provided the best fit for the adsorption kinetics of the WsBio-LDH composite. FTIR spectra revealed various functional groups on the surface of the WsBio-LDH composite before and after Cu^{2+} adsorption. The SEM images indicated a rough surface with two distinct phases of raw biochar andcu micro-sized Ca/Al/Mg-LDH particles, and roughness enhances further after the Cu^{2+} adsorption. EDX analysis further confirms the adsorption of Cu^{2+}. These results underscore the efficacy of the WsBio-LDH composite as a promising nano-adsorbent for wastewater treatment applications.

Keywords: Copper removal, Monolayer adsorption, RSM optimization, WsBio-LDH composite.

Received: 07/10/2025,

Accepted: 11/06/2026,

Available online: 02/07/2026

Graphical abstract

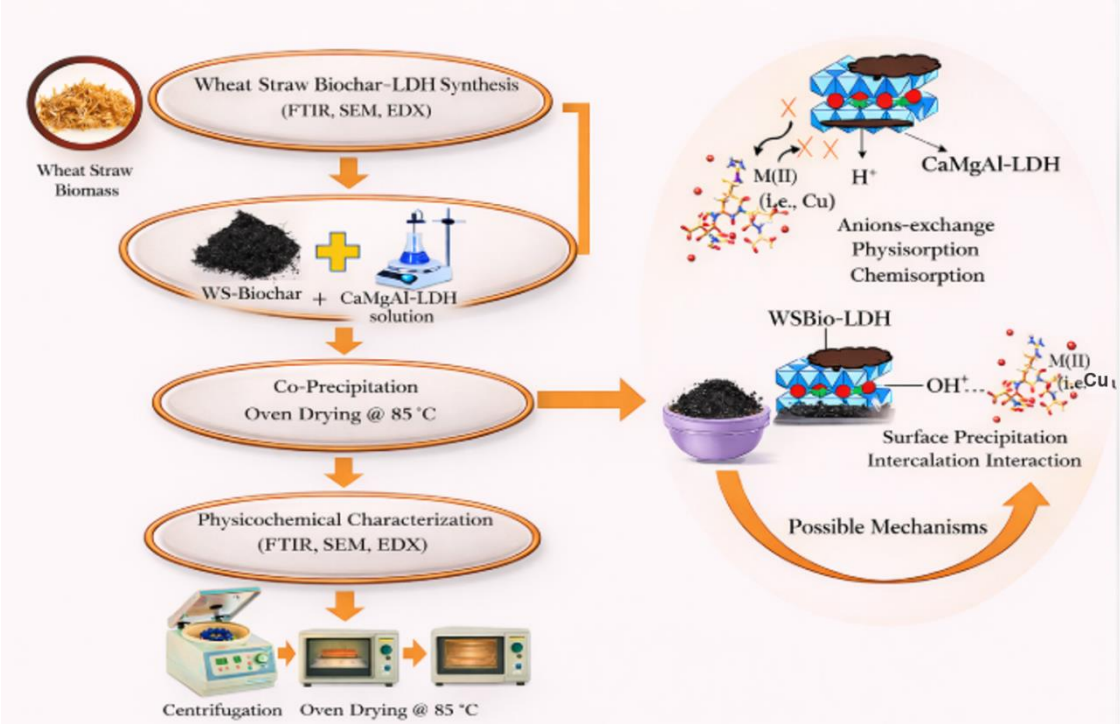

1. Introduction

The need for clean water for everyday use is rising because of the fast expansion of the population, commercialization, and civilization. Global concerns regarding heavy metal pollution have gained significant attention in recent years due to their toxicity and bioaccumulation potential. Industrial effluents and the discharge of untreated sanitary waste are ranked as the primary sources that contribute to heavy metals pollution of aquatic environment (Bej *et al.* 2023). Heavy metals are non-biodegradable and hence persistent in aquatic environments (Biswal and Balasubramanian 2023). Among heavy metals, copper (Cu^{2+}) is the most harmful pollutant, which usually enters water systems through various industrial processes such as mining, battery manufacturing, and paint production. Cu^{2+} contamination induces extreme health risks, such as neurological damage and developmental disorders (Gaetke *et al.* 2014). It also causes gastrointestinal distress with short-term exposure, while liver or kidney damage may occur with long-term exposure. Therefore, it is direly needed to treat Cu^{2+} loaded effluents prior to disposal freshwater environment. Many treatment strategies, including membrane filtration (Mokhtar *et al.* 2018), ion exchange resin (Zakaria *et al.* 2023), coagulation (Luo *et al.* 2018) and flocculation (Sun *et al.* 2022) have been applied to remove Cu^{2+} from waste streams. Various technologies, including membrane-based extraction processes, have been investigated for the removal of heavy metals from aqueous solutions (Fouad *et al.* 2017). However, membrane fouling (Al-Rashdi *et al.* 2013), high working costs of ion exchange resins (Hagag *et al.* 2017), Cu^{2+} rich sludge generation and secondary pollution (Kouniba *et al.* 2024), Cu^{2+} recover from sludge (Trinh *et al.* 2021) and undesired retention of ions in ultrafiltration (Gräf *et al.* 2023) are recognized drawbacks of these techniques. Advanced functional materials have also been investigated for wastewater treatment applications. Recent studies reported that nonstoichiometric Mn–Co spinel oxides effectively activate oxidants for the removal of organic pollutants in continuous-flow wastewater treatment systems, demonstrating the importance of engineered materials for environmental remediation (Liang *et al.*2026). Recent studies have also demonstrated the effectiveness of advanced engineered materials for wastewater remediation. For example, visible-light-activated $CuFe_2O_4$/Zn-BTC photocatalysts have shown efficient mineralization and detoxification of hazardous contaminants in industrial effluents, highlighting the growing importance of multifunctional materials for environmental treatment applications (Mahmood *et al.* 2026) Resource recovery and contaminant removal have become important objectives in modern wastewater treatment systems. Recent investigations have demonstrated simultaneous pollutant degradation and nutrient recovery using advanced oxidation processes, emphasizing the growing need for sustainable remediation technologies (Wang *et al.* 2026). On the other hand, adsorption presents as the best alternative due to its low cost, ease of application, efficiency even at low concentrations, and environmentally friendly technique (Akhtar *et al.* 2025). Adsorption is an efficient process because it can remove several pollutants, including biological and inorganic substances, which contain soluble and non-soluble compounds from wastewater without

producing toxic substances (Rashid *et al.* 2021). Various adsorbents such as metal oxides (Liu and Wang 2013a), metal organic framework (Han *et al.* 2024), steel slag (Mingming *et al.* 2023), Modified adsorbent hydroxypropyl cellulose xanthate (Zhang *et al.* 2016), and synthetic abalone shell hydroxyapatite microspheres (Wang *et al.* 2022) have been explored in the literature for Cu^{2+} removal. However, naturally occurring adsorbents derived from bio-resources offer significant advantages, including abundance, low cost, and environmental sustainability (Dehghani *et al.* 2023).

Recent advances have demonstrated the role of intelligent and hybrid modeling approaches in environmental remediation. For example, Internet of Things (IoT) enabled Recurrent Neural Network (RNN) and Graph Neural Networks (GNN) based systems have been applied for real-time wastewater monitoring and agricultural sustainability (Alprol *et al.* 2024; Tabassam *et al.* 2025). The development of economical and sustainable water reclamation systems has further emphasized the need for efficient treatment materials capable of removing contaminants at low operational cost (Syed et al, 2024). Although these studies focus on sensor-based intelligence, material level innovations such as the WsBio-LDH composite remain essential for effective pollutant removal, highlighting the complementary role of advanced adsorbents in smart water treatment frameworks (Das *et al.* 2025).

Recent progress in sustainable environmental technologies has also emphasized the importance of understanding material-level reaction mechanisms and surface interactions. For instance, mechanistic studies on CO_2 conversion systems have demonstrated that catalyst surface properties and interfacial reactions play a crucial role in determining pollutant transformation efficiency and process performance (Hussain *et al.* 2026). Although the present work focuses on Cu^{2+} adsorption rather than catalytic CO_2 conversion, both fields highlight the significance of rational material design and surface engineering for improving environmental remediation technologies.

In recent years, globally agriculture has produced millions of tons of agricultural bioresources, including wheat straw (WS), which is ranked as the second largest lignocellulosic material (Riseh *et al.* 2024). Every year, crop waste is burned in fields, releasing a variety of pollutants in the environment, like CO, particulate matter, and unburned hydrocarbons, and it is a common practice worldwide. Consequently, environmental pollution increases, and valuable bioresources are wasted. Therefore, it is imperative to transform agricultural waste into wealth through value addition (Priya *et al.* 2025) and, importantly, to reduce pollution.

The growing emphasis on sustainable material development has encouraged the adoption of green processing technologies and environmentally benign modification strategies across various industrial sectors. Recent advances in deep eutectic solvent-based material modification have demonstrated the potential of green chemistry approaches for enhancing material functionality while minimizing environmental impacts (Farooq *et al.* 2025). Such developments further support the need for sustainable adsorbent design for wastewater remediation.

The sustainable utilization of biomass and agricultural residues has gained increasing attention as part of the circular economy concept. Recent studies have emphasized that waste-derived resources can serve as valuable feedstocks for environmental and energy-related applications, reducing disposal problems while creating economic and environmental benefits (Hassan *et al.* 2023, Li *et al.* 2025). In this context, wheat straw represents an abundant agricultural residue that can be converted into value-added biochar-based materials for wastewater treatment.

As a renewable natural resource, WS offers significant potential to produce biochar, which can be utilized in various environmental applications. Biochar is a carbon-rich solid byproduct produced through the pyrolysis of biomass at temperatures below 700°C. It can be derived from a wide range of low-cost biomass sources, including manure (Cao *et al.* 2009), organic waste (Kumar *et al.* 2016), bioenergy crops (e.g., grasses and willows) (Yrjälä and Zheng 2021), and crop residues (Patel and Panwar 2023). Recent bioresource valorization studies have further highlighted the environmental benefits of converting biomass into biochar and other value-added products for sustainable applications (Tanweer *et al.* 2025). Biochar's physicochemical properties, like a large surface area, high porosity, abundant oxygen-rich functional groups, and notable cation exchange capacity, make it a highly effective adsorbent for wastewater treatment in comparison to metal based adsorbent (Hussain *et al.* 2025; Johnston *et al.* 2021). The presence of oxygenated functional groups on the biochar surface imparts a negative charge, facilitating the adsorption of positively charged heavy metals and other pollutants from wastewater (Zhang *et al.* 2025). As a result, it is suitable for use as an adsorbent material to reduce the levels of heavy metals in water. Additionally, biochar can reduce environmental pollution, enhance soil quality (Kabir *et al.* 2023), promote sustainability (Afshar and Mofatteh 2024) and slow down climate change (Shoudho *et al.* 2024). Numerous studies have demonstrated the effectiveness of biochar as a cost-efficient and highly capable adsorbent for wastewater treatment, alongside its applications in soil improvement.

Biomass-derived biochar has been widely proposed for the removal of various contaminants from water, including organic pollutants, heavy metals, and nutrient pollutants (Elbagory *et al.* 2025; Liu *et al.* 2025; Ma *et al.* 2025; Olugbenga *et al.* 2024; Yan *et al.* 2025). Recent studies have further demonstrated that biomass-derived porous carbon materials exhibit excellent adsorption performance toward emerging contaminants due to their high surface area, hierarchical pore structure, and abundant functional groups. For instance, lignin-derived hierarchical porous carbon showed enhanced adsorption capacity for tetracycline, highlighting the potential of biomass-based adsorbents for environmental remediation (Li *et al.* 2026). One of the studies reported the removal of Cu^{2+} by WS

biochar, which showed 6.6% at pH 4.5 and 20.12% at 8 g dose (Wang *et al.* 2022). However, W-S biochar is often limited by its surface chemistry and adsorption capacity. To overcome these limitations, biochar modifications have been explored to enhance its adsorption properties. One approach is to incorporate layered double hydroxides (LDHs), such as calcium-magnesium-aluminum (Ca–Mg–Al) LDH, onto biochar. LDHs are known for their high anion-exchange capacity, tunable composition, and interlayered structure, which facilitate the adsorption of various contaminants (Kameliya *et al.* 2023). When combined with biochar, these properties may create a material with synergistic effects.

As previously mentioned, WS a plentiful agricultural byproduct, offered a cheap and renewable precursor for the creation of biochar. For Cu^{2+} ion adsorption under batch conditions, the Ca–Mg–Al LDH modified wheat straw biochar (WsBio-LDH composite) was optimized. By employing commonly used isotherms, such as Langmuir, Freundlich, and Temkin, as well as kinetic models, such as pseudo-first-order (PFO) and pseudo-second order (PSO), the mechanism of Cu^{2+} ion adsorption by the WsBio-LDH composite was examined. In order to achieve optimal experimental settings, response surface methodology (RSM) with a central composite design (CCD) were also used to determine optimal experimental conditions and analyze the interactive effects of operational parameters.

This study contributes to ongoing research on sustainable adsorbent development for environmental remediation. The present work explores the integration of Ca–Mg–Al layered double hydroxides (LDHs) with wheat straw biochar to prepare a biomass-derived composite adsorbent for Cu^{2+} removal. Response surface methodology based on central composite design (RSM-CCD) is further applied to optimize key adsorption parameters and support the interpretation of process–performance relationships. The increasing interest in sustainable material engineering has extended across several environmental fields, including wastewater remediation, carbon utilization, and clean energy production. Recent studies have emphasized the role of tailored material structures and surface-active sites in enhancing environmental performance. However, the combined use of wheat straw biochar and Ca–Mg–Al LDHs for Cu^{2+} removal under statistically optimized conditions remains relatively underexplored. Therefore, this study aims to address this gap by preparing a wheat straw biochar-supported Ca–Mg–Al LDH composite and evaluating its adsorption performance through a systematic RSM-CCD approach.

2. Materials and Methods

2.1. *Synthesis of LDH W-S Biochar Composite*

The co-precipitation method was used to prepare the composite adsorbent of CaMgAl(LDH) and WS biochar. To prepare the LDH of CaMgAl, 5.90 g (0.5 M) of calcium nitrate tetrahydrate $Ca(NO_3)_2{\cdot}4H_2O$, 6.025 g (0.5 M) of aluminum nitrate nonahydrate $Al(NO_3)_3{\cdot}9H_2O$, and 6.41 g (0.5 M) of magnesium nitrate hexahydrate $Mg(NO_3)_2{\cdot}6H_2O$ were dissolved in 50 mL of deionized water in a beaker. The mixture was stirred continuously for about an hour to ensure complete dissolution of the salts. Once dissolved, the solution was transferred to another beaker containing 5 g of WS biochar, and the mixture was stirred continuously. A solution of NaOH (0.42 g) and Na_2CO_3 (0.58 g) in 100 mL of deionized water was then added dropwise via a burette until the pH of the solution reached approximately 10. The resulting slurry was stirred for an additional two hours. Afterward, the slurry was transferred to a centrifuge tube and centrifuged at 6000 rpm to separate the particles. This washing step was repeated five times using deionized water. Following the washing procedure, the composite material was dried in an oven at 85°C for 24 hours.

2.2. *Batch Adsorption Experiment*

Batch adsorption experiments were performed to evaluate the removal of Cu^{2+} from aqueous solution using the WsBio-LDH composite as an adsorbent. Stock solutions of Cu^{2+} were prepared at a concentration of 20 ppm. For each experiment, an appropriate dose of the adsorbent (0.4 g) was added to 40 mL of the Cu^{2+} solution in a flask. The pH of the solutions was adjusted to 6.0 using 0.1 M HCl and 0.1 M NaOH, as needed (Mondal 2009). The mixture was mechanically shaken at a speed of 200 rpm at ambient temperature (25°C) using an orbital shaker to ensure uniform mixing. At regular time intervals, the residual concentrations of Cu^{2+} in the solutions were analyzed using the Atomic Absorption Spectrometer. The residual Cu^{2+} concentration at time (t) was calculated using the following equation:

$$q_t = \frac{C_0 - C_t}{m} \times V \tag{1}$$

In this equation, V (mL)' represents the volume of solution, and m (g) corresponds to the mass of the WsBio-LDH composite. 'C_0' is the initial metal ion concentration (mg/L), 'C_t' is the metal concentration at time t (mg/L) (Bayantong *et al.* 2021).

The % removal efficiency of the adsorption process was calculated using Equation 2.

$$\%\ \text{removal} = \frac{C_0 - C_t}{C_0} \times 100 \tag{2}$$

Other batch parameters were also tuned, including the dose of the WsBio-LDH combination, the starting concentration of Cu^{2+}, and the pH of the solution. Isotherms and kinetic models were used to examine the WsBio-LDH composite's chemical and physical surface properties as well as Cu^{2+} molecules' affinity for the adsorbent's surface coverage. The adsorption of Cu^{2+} was investigated using the Langmuir, Freundlich, and Temkin isotherm models, which looked at the interactions between the adsorbent and the investigated metal ions at various concentrations.

2.3. *Isotherm Models*

The linear representation of the Freundlich isotherm is depicted in Equation 3, where K_f represents the Freundlich

constant and 1/n denotes the adsorption intensity, which depends on the heterogeneous nature of the nanocomposite (Cheung *et al.* 2007a; Liu and Wang 2013a). The Freundlich isotherm is formulated under the assumption of a heterogeneous surface (Othman *et al.* 2023) with a non-uniform distribution of active sites over the surface through a multilayer adsorption process. The value of 1/n determines the isotherm type, in which 1/n = 0, 0 < 1/n < 1, and 1/n > 1 indicate irreversible, favorable, and unfavorable adsorption, respectively.

$$logq_e = logK_f + \frac{1}{n} logC_e \quad (3)$$

The Freundlich isotherm equation was applied to describe multilayer adsorption on heterogeneous surfaces (Cheung *et al.* 2007b; Liu and Wang 2013a). According to the Langmuir model, the surface of the adsorbent possesses a predetermined number of active sites where the adsorbate can adhere to form a monolayer. Once a monolayer has formed, no additional adsorbate can adhere to the surface. The linear form of the Langmuir model is shown in Equation 4. C_e (mg/L) shows the liquid phase concentration, where qe (mg/g) denotes the adsorption capacity of the WsBio-LDH composite at equilibrium. By plotting 1/qe against 1/Ce, it is possible to obtain the value of K_L. K_L (L/g) is the Langmuir isotherm constant, and q_{max} signifies the maximum adsorption capacity related to the area occupied by a monolayer of adsorbate.

$$\frac{1}{q_e} = \left(\frac{1}{K_L q_{max}}\right)\frac{1}{C_e} + \frac{1}{q_{max}} \quad (4)$$

The Langmuir model assumes monolayer adsorption on a homogeneous surface with finite adsorption sites (Liu and Wang 2013b). Unlike the Langmuir isotherm, the Temkin isotherm assumes that adsorption energy decreases linearly as adsorbent-adsorbate interaction increases and more surface of the adsorbent is covered with adsorbate molecules. Equation 5 represents the linear form of the Temkin isotherm model, where B = RT/b, b (KJ/mol) represents the Temkin constant, R is known as the universal gas constant (8.314 J mol−1 per kelvin), B shows the heat of adsorption (J/mol), and A is the Temkin constant.

$$q_e = \frac{RT}{B_T}\ln A_T + \frac{RT}{B_T}\ln C_e \quad (5)$$

The Temkin model considers adsorbent adsorbate interactions and a linear decrease in adsorption energy (Othman *et al.*, 2023).

2.4. *Kinetic Models*

The kinetics of adsorption is known as the key to understanding how quickly an adsorbent can capture an adsorbate (metal) from a solution. Various kinetic models are used to interpret the experimental adsorption data and determine the rate-limiting step.

The PFO model assumes that the adsorption rate is directly proportional to the number of unoccupied active sites on the adsorbent. This model is typically applicable to systems where physisorption is the dominant adsorption mechanism. The linear form of the PFO model is expressed in Equation 6

$$\log q_{e-}q_t = logq_e - \frac{k_1}{2.303}t \quad (6)$$

Here, k1 is the PFO rate constant (min^{-1}), q_t is the quantity of metal ion adsorbed at time t (mg/g), and qe is the amount of adsorbate adsorbed at equilibrium (mg/g).

Physisorption-controlled adsorption processes were described by the pseudo-first-order kinetic model (Cheung *et al.*, 2007).

According to the PSO model, the square of the number of vacant sites determines the rate of adsorption. It is frequently employed in chemisorption procedures, in which the adsorbent and adsorbate form chemical bonds. Equation 7 represents the PSO model linear form.

$$\frac{t}{q_t} = \frac{1}{k_2 q^2_e} + \frac{t}{q_t} \quad (7)$$

Here, K_2 is the PSO rate constant (g/(mg/min). The pseudo-second order kinetic model assumes chemisorption as the rate-limiting step (Othman *et al.*, 2023).

Table 1. Independent variables and their coded levels.

Independent variables	Units	+1	0	-1
T	Min	1	60.5	120
LDH/W.B. Dose	g/L	0.05	0.325	0.6
pH		2	4	6
Cu^{+2} Conc.	mg/L	5	37.5	70

2.5. *Characterization Techniques*

Characterization techniques used for the WsBio-LDH composite adsorbent include Fourier transform infrared (FTIR) spectroscopy, the energy dispersive X-ray (EDX) spectroscopy, and scanning electron microscopy (SEM) to investigate the surface functional groups and morphological changes. FTIR analysis was specifically employed to identify the chemical bonds, and functional groups present on the surface of the WsBio-LDH composite adsorbent (Haleem *et al.* 2022), both before and after Cu^{2+} adsorption. SEM and EDX provided a few insights into the surface morphology (Obey *et al.* 2022), revealing structural changes and the adsorption of metal ions, which helped in assessing the effectiveness of the WsBio-LDH composite adsorbent in removing Cu^{2+} from aqueous solution

2.6. *Response Surface Methodology*

The RSM was used to systematically optimize and assess the relationship between adsorption efficiency (response) and the impact of various parameters on the Cu^{2+} removal efficiency of the WsBio-LDH composite (Abdipour and

Hemati 2024; Jafari *et al.* 2025; Torabideh *et al.* 2025) . A quadratic relationship in RSM was constructed using a three-factor CCD. Factorial, axial, and center points are all combined in this model. As indicated in **Table 1**, the main independent factors (along with coded levels) include contact duration, dose of the WsBio-LDH combination, solution pH, and Cu^{2+} concentration, which were examined for their effects on removal efficiency. WsBio-LDH The effects of both individual variables and their interactions on the Cu^{2+} removal efficiency of WsBio-LDH composite's was evaluated.

2.7. *Workflow of the Proposed Experimental Optimization Model*

The proposed study follows a systematic workflow comprising:

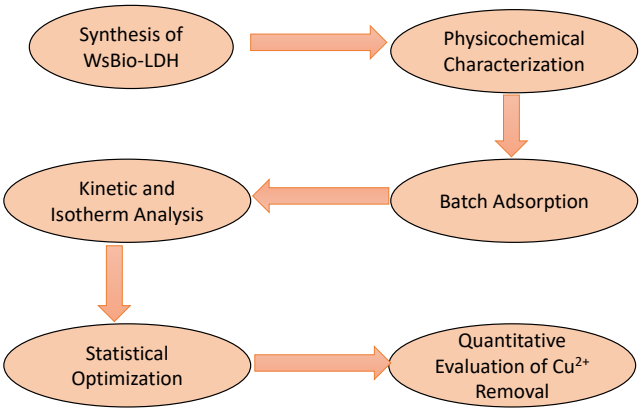

Workflow for the removal of Cu^{+2}

3. Results and Discussions

3.1. *FTIR Spectroscopy*

The FTIR spectra of the WsBio-LDH composite before and after Cu^{2+} adsorption are presented in **Figure 1**, illustrating the changes in surface functional groups. The bands seen at 3389 and 1637 cm^{-1} are linked to the typical -OH stretching vibrations and the bending vibrations of H_2O (Xu *et al.* 2020). These are related to the hydroxyl groups found in the adsorbent, as well as the water that is either adsorbed or located between the layers of the sorbent. The characteristic peaks at 2093 cm^{-1} indicate the presence of C≡C or C≡N stretching vibrations, suggesting unsaturated alkyne. The sharp peaks at 1328 and 991 cm^{-1} were allocated to the asymmetric stretching vibration mode of C–O in CO_3^{2-} and stretching of C-O, respectively (Adachi-Pagano *et al.* 2003; Zou *et al.* 2017).

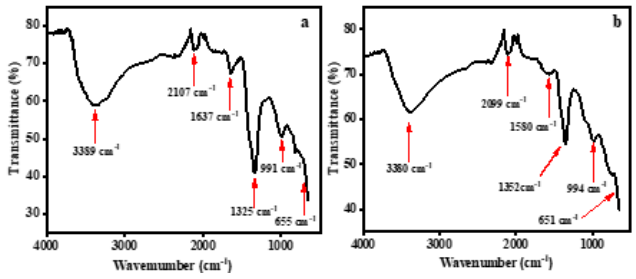

Figure 1. Fourier transform infrared spectra of (a) the WsBio-LDH composite, and (b) the WsBio-LDH composite after Cu^{2+} adsorption.

The bands about 655 cm^{-1} are associated with M-OH or M-O stretching vibrations, where M represents Mg, Al, or Ca. The relationships between cations and oxygen are defined by these bands (Frost and Kloprogge 1999). Following the Cu^{2+} adsorption, the FTIR spectra of the WsBio-LDH composite exhibit a discernible shift, as shown in **Figure 1b**. Cu^{2+} was successfully adsorbed onto the surface of the WsBio-LDH composite adsorbent, as evidenced by the shift of all the bands and the narrowing of the OH band. The signal at 1637 cm^{-1} is reduced and shifted to 1580 cm^{-1} by the Cu^{2+} interaction, indicating a decrease in hydroxyl frequency (Chen *et al.* 2024). The consumption of hydroxyl groups during the adsorption process could be attributed to the formation of Cu-OH on the surface of the WsBio-LDH composite (Lyu *et al.* 2023).

3.2. *Scanning Electron Microscopy*

Figure 2 illustrates the use of SEM and EDX analyses to examine the surface shape and elemental composition of the WsBio-LDH composite before and after Cu^{2+} adsorption. SEM imaging enables visualization of surface modifications, facilitating a better understanding of morphological changes (Rydz *et al.* 2019). As seen in Figure 2a (Shiriazar *et al.* 2022), SEM scans revealed a rough surface of the WsBio-LDH composite that primarily contained two separate phases: the raw biochar and micro-sized Ca/Al/Mg-LDH particles scattered over it. Cu^{2+} is successfully adsorbed into the WsBio-LDH composite adsorbent, as seen in Figure 2b, where the holes become saturated with Cu^{2+} and the surface of the WsBio-LDH composite appears rougher.

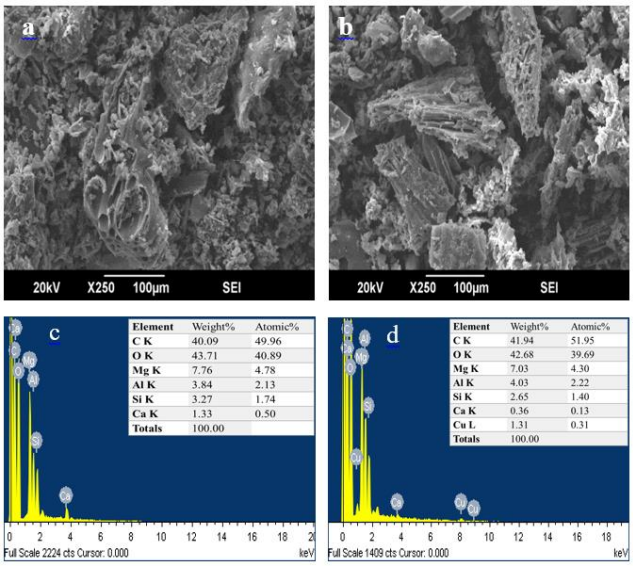

Figure 2. SEM images of (a) the WsBio-LDH composite, and (b) the WsBio-LDH composite after Cu^{2+} adsorption. EDX spectra of (c) the WsBio-LDH composite and (d) the WsBio-LDH composite after Cu^{2+} adsorption.

EDX spectroscopy showed the elemental composition of the WsBio-LDH composite before and after adsorption of Cu^{2+} (Nzediegwu *et al.* 2021). As shown in Figure 2c, an increase in oxygen content (70.62 wt%) and a reduction in carbon content (17.07 wt %) were observed, implying successful adsorption and surface modification. Furthermore, in the WsBio-LDH composite, peaks

corresponding to Ca, Al, and Mg confirmed successful inclusion of these elements. Subsequently, the WsBio-LDH composite displayed changes in elemental distribution and the presence of Cu^{2+} ions (Figure 2d), which demonstrates the interactions between the Cu^{2+} and the surface of the WsBio-LDH composite.

3.3. *Effect of Adsorption Parameters*

3.3.1. Effect of the Contact Time

Figure 3 illustrates the effect of contact time on Cu^{2+} removal efficiency and adsorption capacity of the WsBio-LDH composite. Determination of contact time aims to get the optimum time to adsorb contaminants. In this study, time variations were used as 1, 5, 10, 15, 30, 60, 100, and 120 minutes, and the effect of contact time was studied at room temperature along with 0.4 g of the WsBio-LDH composite adsorbent for Cu^{2+} removal. Figure 3 shows that the WsBio-LDH composite revealed better performance, achieving 98.6% removal at 60 minutes, which increased slightly to 99% at 120 minutes. These results clearly indicate that the WsBio-LDH composite is significantly more effective for Cu^{2+}+ removal. Therefore, 60 minutes contact time was selected as the optimum time for further experiments, i.e., pH, Cu^{2+} concentration, and dose effect on %age removal of the studied adsorbate (Cu^{2+}).

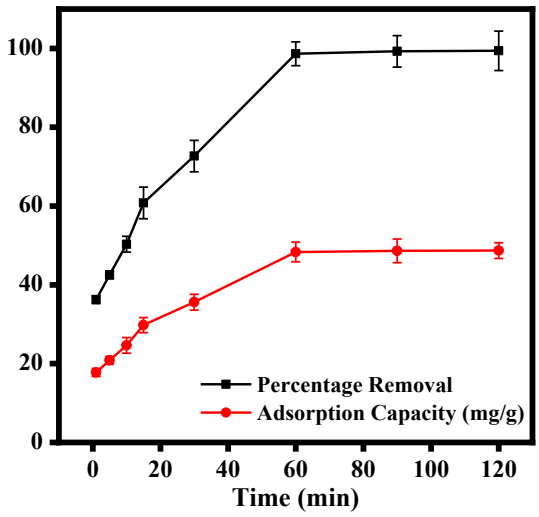

Figure 3. Effect of the contact time on the adsorption capacity and % removal of the WsBio-LDH composite for Cu^{2+} ions from aqueous solution.

It should be noted that the contact-time experiment was conducted independently to determine the equilibrium behavior of the adsorption process under fixed operating conditions. Although Cu^{2+} removal reached approximately 98.6% within 60 min, the RSM optimization considered the simultaneous interactions among contact time, adsorbent dosage, solution pH, and initial Cu^{2+} concentration. Consequently, the statistically optimized contact time predicted by the RSM model was 87.06 min, which corresponds to the maximum overall removal efficiency obtained when all process variables were optimized together. Therefore, the values of 60 min and 87.06 min are not contradictory but represent single-factor and multi-factor optimization outcomes, respectively.

The adsorption kinetics of Cu^{2+} onto the WsBio-LDH composite were analyzed using pseudo-first-order (PFO), pseudo-second-order (PSO), and intraparticle diffusion (IPD) models, as presented in Figure 4, with the corresponding kinetic parameters summarized in **Table 2**.

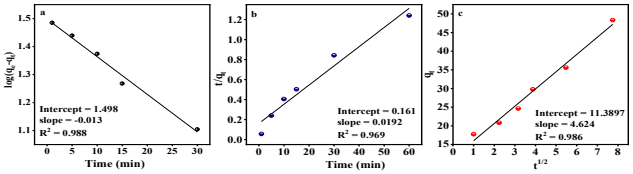

Figure 4. Kinetic model analysis for the WsBio-LDH composite (a) PFO, (b) PSO, (c) IPD.

The adsorption kinetics of Cu^{2+} onto the WsBio-LDH composite were evaluated using both pseudo-first-order (PFO) and pseudo-second-order (PSO) models. The PFO model exhibited a slightly higher coefficient of determination (R^2 = 0.988) compared with the PSO model (R^2 = 0.969), indicating a better statistical fit to the experimental data. Therefore, based solely on the R^2 values, the PFO model more accurately describes the adsorption kinetics . However, the relatively high R^2 values obtained for both models suggest that the adsorption process may involve contributions from both physical and chemical interactions between Cu^{2+} ions and the WSbio-LDH surface. The observed agreement with the pseudo-first-order model suggests that physisorption may contribute significantly to the adsorption process. Similar adsorption behavior governed by physical interactions has been reported for pollutant adsorption systems involving surface-mediated adsorption mechanisms (Qin *et al.* 2023).

Table 2. Kinetic model parameters for adsorption of Cu^{2+} on WsBio-LDH composite.

Kinetic models	Parameters	Values for the WsBio-LDH composite
PFO	K_1	0.03
	q_{exp}	48.3
	q_{cal}	52.63
	R^2	0.986
PSO	K_2	0.0022
	q_{exp}	48.3
	q_{cal}	52.63
	R^2	0.969
IPD	I	11.39
	k_{diff}	4.62
	R^2	0.988

3.3.2. Effect of the Adsorbent Dose

Figure 5 illustrates the effect of WsBio-LDH composite dose on the adsorption capacity and removal efficiency of Cu^{2+}. The adsorbent dosage regulates the accessibility of adsorption (Wang *et al.* 2020). The adsorbent's dosage was adjusted in increments of 0.1 g between 0.05 and 0.6 g under the following conditions: at an initial pH of 6, a contact period of 60 minutes, a shaking speed of 200 rpm, and room temperature. Figure 5 illustrates how the proportion of Cu^{2+} ions eliminated increased with an increase in adsorbent dosage. As seen, the percentage removal of Cu^{2+} reached 98% at 0.4 g of adsorbent used and increased to 100% at 0.6 g for the WsBio-LDH combination. These results demonstrate that increasing the adsorbent dosage enhances the adsorption efficiency, likely due to the increased accessibility of active adsorption sites.

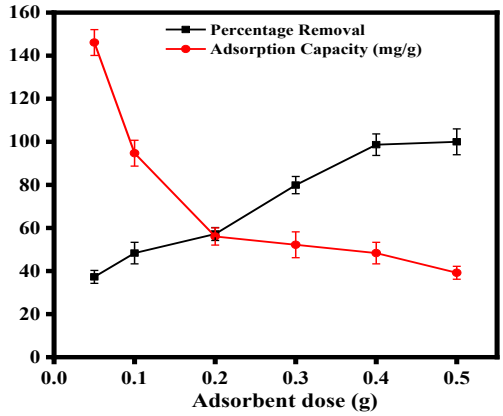

Figure 5. Effect of the WsBio-LDH composite dose on the adsorption capacity and Cu^{2+} % removal.

3.3.3. Effect of the Cu^{2+} Concentration

Figure 6 show that the initial Cu^{2+} concentration affects the WsBio-LDH composite adsorption ability. Figure 6 shows the percentage removal of Cu^{2+} metal ions for the WsBio-LDH composite adsorbent at different starting concentration levels ranging from 5 to 70 mg/L. The results indicate that as the concentration of the adsorbate increased, the percentage removal of the metal ions under study decreased. The accessible empty binding sites on the adsorbent's surface are responsible for the increased Cu^{2+} absorption at lower concentrations. The increased Cu^{2+} metal ion in the aqueous phase results in competition and saturation on the adsorbent surface, which is responsible for the decrease in the percentage of metal removal. Thus, mass transfer is hampered (El-Shafey *et al.* 2024).

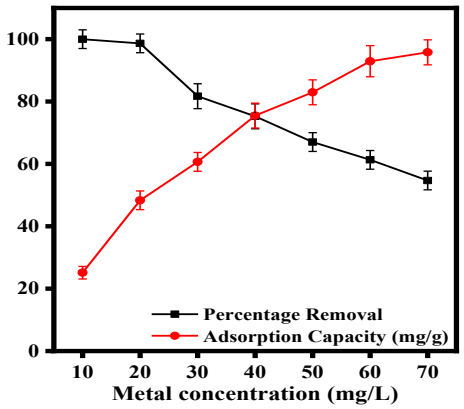

Figure 6. Effect of initial Cu^{2+}concentrations on the adsorption capacity and % removal of Cu^{2+} using the WsBio-LDH composite as an adsorbent.

3.4. *Adsorption isotherms*

The adsorption behavior of Cu^{2+} onto the WsBio-LDH composite was evaluated using Langmuir, Freundlich, and Temkin isotherm models, as shown in Figure 7, with the corresponding isotherm parameters summarized in **Table 3**. The Langmuir model provided the best fit, with a higher R^2 value of 0.997 for the WsBio-LDH composite. Additionally, the adsorption capacity increased, as seen in **Table 3** for the WsBio-LDH composite, indicating that the modification has enhanced the adsorption efficiency, and the adsorption process follows a monolayer adsorption mechanism.

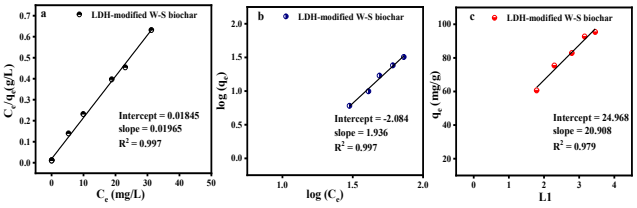

Figure 7. Adsorption isotherms: (a) Langmuir isotherm, (b) Freundlich isotherm, and (c) Temkin isotherm for Cu^{2+} adsorption on the WsBio-LDH composite.

Table 3. Isotherm model parameters of Cu^{2+} adsorption on WsBio-LDH composite.

Isotherm models	Parameters	Values for the WsBio-LDH composite
Langmuir	q_{exp}	95.79
	q_{max}	100.00
	R_L	0.02
	R^2	0.997
Freundlich	K_f	86.10
	N	2.084
	R^2	0.989
	B	120.54
Temkin	LN(AT)	1.194
	R^2	0.979

The Freundlich model, although showing a good R^2 value of 0.989, does not fit the adsorption behaviors as accurately as the Langmuir model in this case. The Temkin model is less suitable for the WsBio-LDH composite adsorbent, especially when compared to the better fits provided by Langmuir and the Freundlich models. In conclusion, the Langmuir model is the best fit, with an increase in adsorption capacity, demonstrating a more favorable monolayer adsorption process for the WsBio-LDH composite.

3.4.1. Effect of the Solution pH

Figure 8 illustrates the effect of solution pH on the Cu^{2+} removal efficiency of the WsBbio–LDH composite at pH values ranging from 2 to 6. Using the WsBio-LDH composite as an adsorbent, 98.6% of the Cu^{2+} was removed at pH 6. This significant improvement in performance highlights the WsBio-LDH composite's greater adsorption capacity and outstanding efficacy in Cu^{2+} removal across the pH range. The percentage of metal ions removed increases as pH rises, according to similar findings reported in the literature (Wang *et al.* 2013). An increase in the percent removal at higher pH is due to less competition by H^+ ions and more efficient de-protonation of functional groups on the surface of the WsBio-LDH composite for copper ion binding.

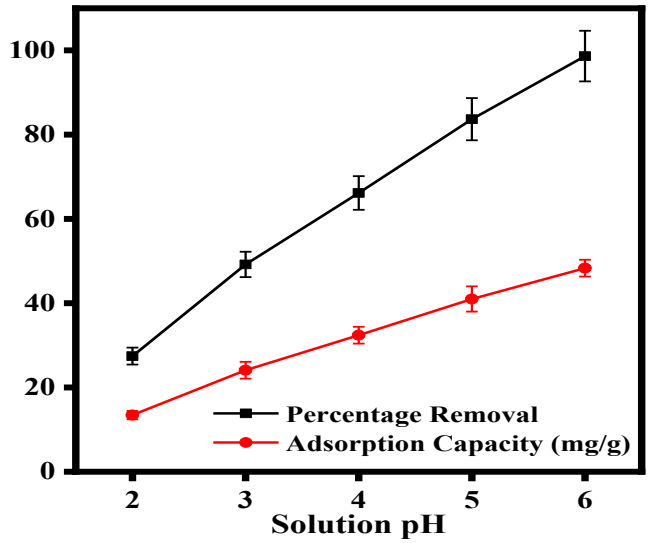

Figure 8. Effect of pH on the adsorption capacity and % removal of Cu^{2+} using the WsBio-LDH composite adsorbent.

3.5. *RSM Analysis of the WsBio-LDH composite vs Cu^{2+} Adsorption*

Response surface methodology was employed to investigate the interactive effects of contact time, adsorbent dosage, solution pH, and initial Cu^{2+} concentration on removal efficiency (Figures 9 and 10). ANOVA results revealed that pH and adsorbent dosage had the most significant positive effects on Cu^{2+} removal efficiency, whereas initial metal concentration negatively impacted removal due to active site saturation. To visualize these effects and their interactions, three-dimensional response surface plots and corresponding contour plots were generated. These graphical representations provide critical insights into the adsorption behavior of the WsBio-LDH composite for Cu^{2+} under varying experimental conditions. Figure 9 (a, b, c) illustrates how changes in the four independent variables, contact time, adsorbent dosage, solution pH, and initial Cu^{2+} concentration influence the overall removal efficiency.

3.5.1. Effect of the Contact Time and the WsBio-LDH Composite Dose

The three-dimensional surface plots and two-dimensional contour diagrams reveal how contact time and adsorbent dosage work together to enhance Cu^{2+} removal. When both parameters are increased, the removal efficiency rises substantially, reaching approximately 90–99% at optimal conditions. Initially, extending the contact duration allows more Cu^{2+} ions to interact with the available active sites on the WsBio-LDH composite surface. This extended interaction period facilitates adequate time for both mass transfer processes and chemical adsorption to occur. Simultaneously, increasing the amount of WsBio-LDH composite introduces additional binding sites into the system. However, the response curves begin to level off at higher adsorbent quantities and prolonged contact periods, suggesting that saturation has been achieved. Beyond a certain threshold, adding more adsorbent or extending the contact time yields minimal improvement in removal performance, likely because active sites begin to overlap or the system reaches equilibrium. These observations align with established adsorption kinetic principles and highlight the effectiveness of LDH functionalization in enhancing the available surface area for adsorption.

3.5.2. Effect of Contact Time and Solution pH

Figure 9b illustrates a interactive effect of pH and contact time. The adsorption efficiency dramatically rises up to roughly 6, after which the curve flattens. At lower pH values (acidic media), the removal efficacy is reduced due to competition between H^+ and Cu^{2+} ions for adsorption sites. As pH approaches neutral, there is less competition and more negative charge density on the adsorbent surface, which promotes Cu^{2+} binding via electrostatic attraction and surface complexation.

When combined with extended contact time, this optimal pH range (5.5-6.5) enables nearly complete Cu^{2+} removal, underscoring the importance of surface chemistry and ionic equilibrium. It is crucial to carefully interpret pH measurements over 7 in these systems because Cu^{2+} precipitates as hydroxides at pH 7, which may impede the actual adsorption mechanism.

3.5.3. Effect of Contact Time and Initial Cu^{2+} Concentration

Particularly at shorter contact durations, this collection of graphs shows an inverse connection between Cu^{2+} concentration and removal efficiency. Cu^{2+} ions compete more fiercely for a small number of adsorption sites as the initial metal concentration rises. This lowers removal efficiency at shorter contact times by limiting the number of active sites available for all ions.

Longer contact times, however, bring the system closer to adsorption equilibrium, allowing for improved removal

even at larger concentrations. However, because the adsorbent surface eventually becomes saturated, achieving maximum efficiency is more difficult than with lower concentrations. For optimal treatment efficacy, these graphs highlight the necessity of optimizing both contact time and Cu^{2+} loading.

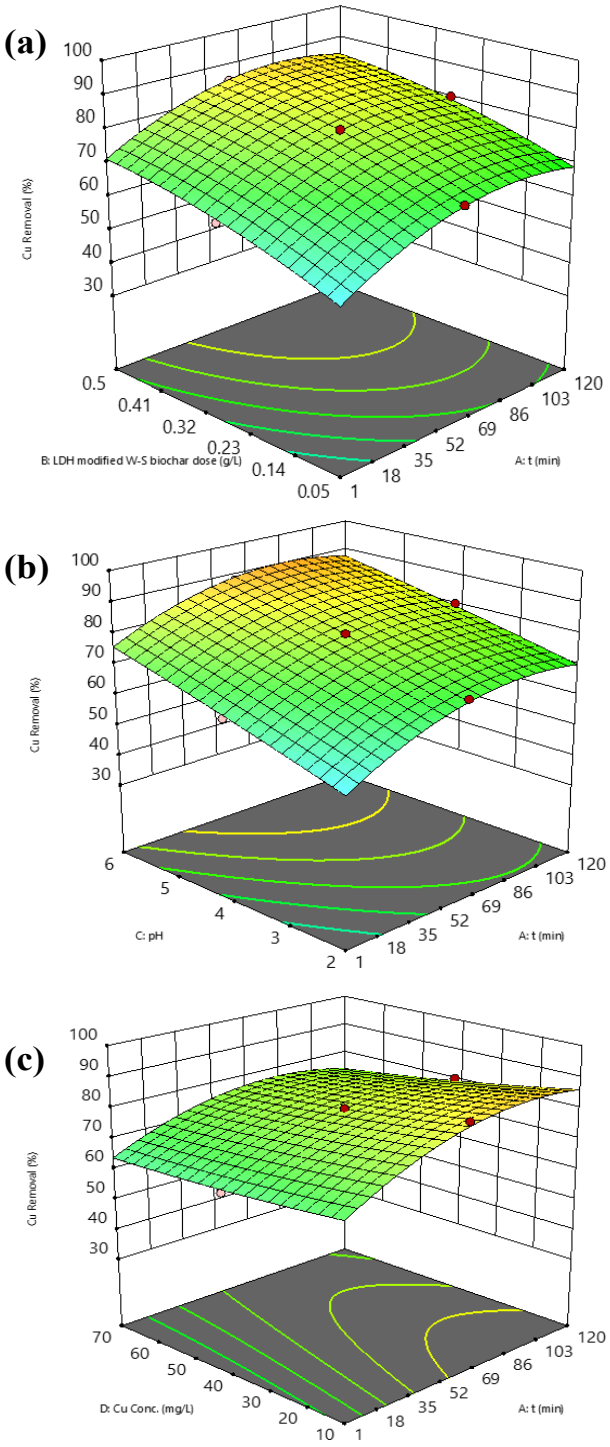

Figure 9. RSM of the interaction between (a) *t* (min) and the WsBio-LDH composite dose (g), (b) *t* (min) and pH, and (c) *t* (min) and Cu^{2+} concentrations (mg/L) on Cu^{2+} removal (%).

3.5.4. Effect of the Solution pH and the WsBio-LDH Composite Dose

The removal of Cu^{2+} is significantly impacted by the pH-adsorbent dosage relationship. The elimination is extremely sensitive to pH variations at low dosages. The elimination is much increased by raising the pH from 3 to about 6, which supports the process of improved surface ionization and electrostatic contact Because there are many surface locations to compensate for less-than-ideal ionic conditions, higher dosages lessen the system's sensitivity to pH. Interestingly, Peak removal occurs at pH 6 at an adsorbent dosage of 0.5 g, as shown in Figure 10a. This result represents an optimal equilibrium in which electrostatic interactions, surface area, and ion exchange capacity are all maximized.

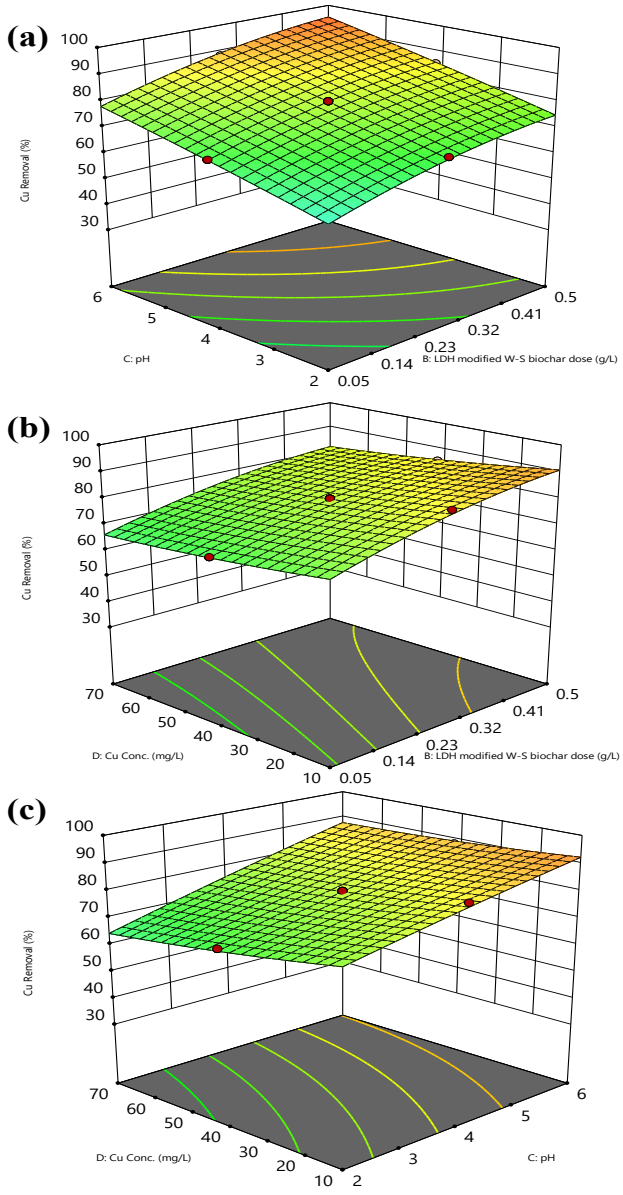

Figure 10. RSM of the interaction between (a) pH and the WsBio-LDH composite dose (g), (b) Cu^{2+} concentrations (mg/L) and the WsBio-LDH composite dose (g), and (c) Cu^{2+} concentration (mg/L) and pH on Cu^{2+} removal (%).

3.5.5. Effect of the Solution pH and Initial Cu^{2+} Concentration

The prominence of pH as a crucial parameter is further demonstrated by the contour and surface plots for pH and Cu^{2+} concentration (Figure 10b). Regardless of Cu^{2+} concentration, elimination improves with increasing pH. However, the effect is stronger at lower concentrations. This implies that when it comes to regulating the adsorption behavior, pH-mediated surface charge alterations are more important than concentration effects.

Due to a lack of active sites and strong competition from H^+ ions, the system performs poorly at low pH and high Cu^{2+} levels. On the other hand, almost total elimination is shown at ideal pH and lower Cu^{2+} concentrations, confirming the need for pH regulation in real-world applications.

3.5.6. Effect of the WsBio-LDH Composite Dose and Cu^{2+} Concentration

The antagonistic relationship between Cu^{2+} concentration and adsorbent dose is depicted in the last set of graphs (Figure 10c). As anticipated, removal efficiency increases with increasing dose, whereas it tends to decrease with rising Cu^{2+} concentration. A higher dose, on the other hand, efficiently counteracts the adverse effects of high concentrations by providing more adsorption sites and protecting the system against abrupt saturation. The system's nonlinear behavior is highlighted by the response surface's curvature, which supports the application of RSM for optimization. Higher adsorbent dosages and lower Cu^{2+} concentrations yield the best results, making them the most important variables to regulate during scale-up or field applications. Figure 11 presents the correlation between actual and predicted values of Cu^{2+} removal using the WsBio-LDH composite adsorbent, while RSM optimized conditions for Cu^{2+} removal using the WsBio-LDH composite adsorbent is shown in Figure 12.

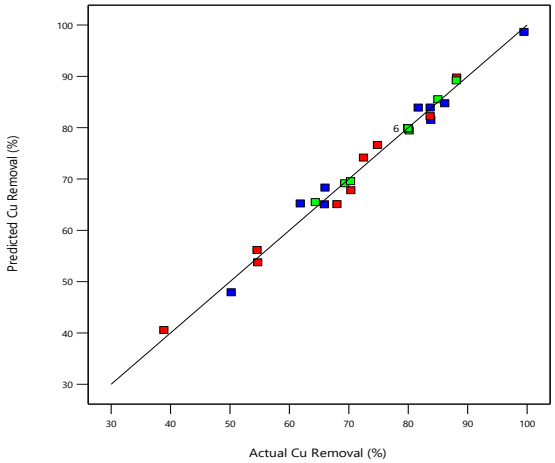

Figure 11. Correlation between actual and predicted values of Cu^{2+} removal using the WsBio-LDH composite adsorbent.

Table 4. Design of experiments and experimental and predicted values for the adsorption efficiency of the WsBio-LDH composite adsorbent against Cu^{2+}.

Run	t (min)	Adsorbent Dose (g)	pH	Cu^{2+} Conc. (mg/L)	Actual Cu^{2+} removal (%)	Predicted Cu^{2+} removal (%)
1	60.5	0.275	4	40	80.00	79.85
2	1	0.05	2	70	38.91	40.54
3	60.5	0.275	4	40	80.00	79.85
4	120	0.5	2	10	81.71	83.88
5	1	0.5	2	70	54.59	56.14
6	60.5	0.275	4	40	80.00	79.85
7	60.5	0.5	4	40	85.02	85.5
8	120	0.05	2	70	54.70	53.73
9	60.5	0.275	6	40	88.12	89.18
10	1	0.05	6	10	61.86	65.2
11	1	0.05	2	10	50.24	47.89
12	120	0.05	6	70	72.50	74.13
13	60.5	0.275	4	40	80.00	79.85
14	60.5	0.275	4	40	80.00	79.85
15	120	0.5	2	70	70.38	67.78
16	1	0.5	2	10	65.92	65.03
17	1	0.5	6	70	83.72	82.2
18	60.5	0.05	4	40	69.34	69.14
19	120	0.05	2	10	66.03	68.29
20	60.5	0.275	4	40	80.00	79.85
21	1	0.5	6	10	83.72	83.89
22	60.5	0.275	4	70	74.85	76.6
23	120	0.275	4	40	80.19	79.42
24	120	0.05	6	10	83.83	81.48
25	60.5	0.275	2	40	70.32	69.55
26	120	0.5	6	70	88.18	89.73
27	1	0.05	6	70	68.04	65.06
28	120	0.5	6	10	99.51	98.62
29	60.5	0.275	4	10	86.18	84.72
30	1	0.275	4	40	64.40	65.46

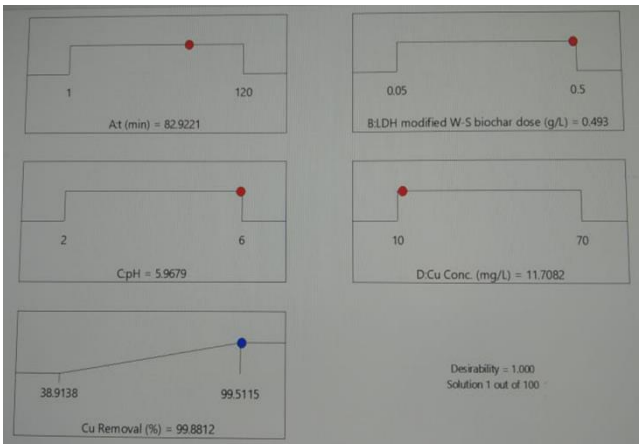

Figure 12. RSM optimized conditions for Cu^{2+} removal using the WsBio-LDH composite adsorbent.

Through RSM technique, the adsorption efficiency of copper ions using the WsBio-LDH composite was thoroughly assessed. The effects of four independent variables, contact time, adsorbent dosage, pH, and initial Cu^{2+} concentration on the adsorption performance were investigated using the BBD. The robustness of the RSM model was validated by the experimental data (**Table 4**), which showed strong consistency with anticipated values. Under optimal conditions, the percentage error was minimum at 0.10 percent. At optimal conditions (87.06 min contact time, 0.491 g WsBio-LDH composite dosage, pH 5.93, and initial Cu^{2+} concentration of 12.75 mg/L), the greatest Cu^{2+} removal efficiency recorded was 99.51% (Table 4). The synergistic interaction between LDH and the WS biochar matrix, which offers a large number of active sites and enhanced surface charge properties at a pH close to neutral, favoring electrostatic interactions with Cu^{2+} ions, is responsible for this high removal efficiency.

Analysis of variance (ANOVA) revealed that the quadratic model was extremely significant ($p < 0.0001$) (**Table 5**). Outstanding model fit and predictability exhibited by its high R^2 value of 0.9854, adjusted R^2 of 0.9719, and predicted R^2 of 0.8839. The four main effects of the independent variables, contact time (A), pH (C), WsBio-LDH composite dose (B), and Cu^{2+} concentration (D), were all statistically significant ($p < 0.0001$), which means that they all affected the adsorption efficiency WsBio-LDH composite for Cu^{2+}. According to the regression model, pH had the biggest positive coefficient (+9.81), followed by adsorbent dose (+8.18) and contact time (+6.98), whereas initial Cu^{2+} concentration had a negative effect (-4.06). These findings imply that while larger initial metal ion concentrations may reduce removal effectiveness due to the saturation of accessible active sites, increasing the pH and dosage significantly improves adsorption.

Table 5. Analysis of variance (ANOVA) for Cu^{2+} adsorption efficiency of WsBio-LDH composite adsorbent.

Model	Quadratic	Significance
Intercept	79.85	
Model P Value	< 0.0001	Significant
A-t	< 0.0001	Significant
B-LDH/W.B. Dose	< 0.0001	Significant
C-pH	< 0.0001	Significant
D-Cu Conc.	< 0.0001	Significant
AB	0.4903	Not significant
AC	0.079	Not significant
AD	0.0049	Significant
BC	0.4903	Not significant
BD	0.4903	Not significant
CD	0.0049	Significant
A^2	< 0.0001	Significant
B^2	0.0818	Not significant
C^2	0.7236	Not significant
D^2	0.5609	Not significant
Lack of Fit	0.6253	Not significant
R^2	0.9854	
Adjusted R^2	0.9719	
Predicted R^2	0.8839	

Table 6. Predicted and observed response values of WsBio-LDH composite for Cu^{2+} under optimized conditions.

Number	t (min)	Adsorbent Dose (g)	pH	Cu^{2+} Conc. (mg/L)	Cu^{2+} Removal (%)		Desirability
1	87.058	0.491	5.927	12.754	Predicted	99.61	1
					Actual	99.51	
					% error	0.10	

The combined influence of these variable pairs appears to have a significant impact on Cu^{2+} uptake, as evidenced by the statistical significance ($p < 0.05$) of interaction terms like AD (contact time and Cu^{2+} concentration) and CD (pH and Cu^{2+} concentration). Notably, a favorable pH at lower concentrations provided ideal binding conditions, whereas

a larger Cu^{2+} concentration combined with a shorter contact period decreased removal efficacy.

Remarkably, the model's accuracy and sufficiency in forecasting the reaction are validated by the non-significant lack of fit (p = 0.6253). These results are further supported by the 3D surface and contour plots (Figure not shown here), which graphically depict the interactions and effects of the factors under study. Finally, the predicted and observed response values of WsBio-LDH composite for Cu^{2+} under optimized conditions are shown in **Table 6** while the model equation can be written as follows;

$$\%\text{Cu removal} = +79.85+6.98A+8.18B+9.81C-4.06D$$
$$-0.3864AB-1.03AC-1.8AD+0.3864BC-0.3864BD+$$
$$1.8CD-7.41A^2-2.53B^2-0.4892C^2+0.8074D^2$$

This work demonstrates the remarkable adsorption ability of the WsBio-LDH composite under ideal circumstances, indicating its potential for effective removal of Cu^{2+} from aqueous solutions. A promising approach to creating affordable, environmentally friendly, and highly effective adsorbents for heavy metal cleanup is the incorporation of LDH into charcoal matrices.

3.6. *Recyclability Performance of the WsBio-LDH Composite*

The reusability performance of the WsBio-LDH composite over multiple adsorption desorption cycles is illustrated in Figure 13. Reusability and stability of the WsBio-LDH composite are critical for practical applications, particularly in wastewater treatment. To evaluate these properties, sorption desorption cycles were conducted over four consecutive experiments. For desorption, 0.1 M HCl was used as the desorption reagent, and agitated it for three hours after adsorption. The results demonstrated the composite exhibited high initial efficiency, with a Cu^{2+} removal rate of 78.7% in the first cycle. However, in the subsequent three cycles, the removal efficiency gradually decreased to 64.6%, 47.4%, and 32.5%, respectively, as shown in Figure 13. This decrease in adsorption efficiency over the cycles may be attributed to the formation of strong chemical interactions among Cu^{2+} ions and the WsBio-LDH composite, which could restrict the regeneration of active sites on the WsBio-LDH composite (Shafiq *et al.* 2025). Despite the slight decrease, the WsBio-LDH composite maintained a high adsorption efficiency of 32.5% after four cycles, demonstrating good stability and reusability, making it a promising candidate for wastewater treatment applications.

The adsorption efficiency decreased progressively from 78.7% during the first cycle to 32.5% after the fourth regeneration cycle. This reduction may be attributed to partial blockage of active adsorption sites, structural alterations of the LDH layers, and incomplete desorption of previously adsorbed Cu^{2+} ions. Although the adsorption capacity declined after repeated use, the composite retained measurable removal capability throughout the regeneration cycles. These findings indicate that further improvements in regeneration procedures and structural stabilization strategies are required to enhance long-term reusability.

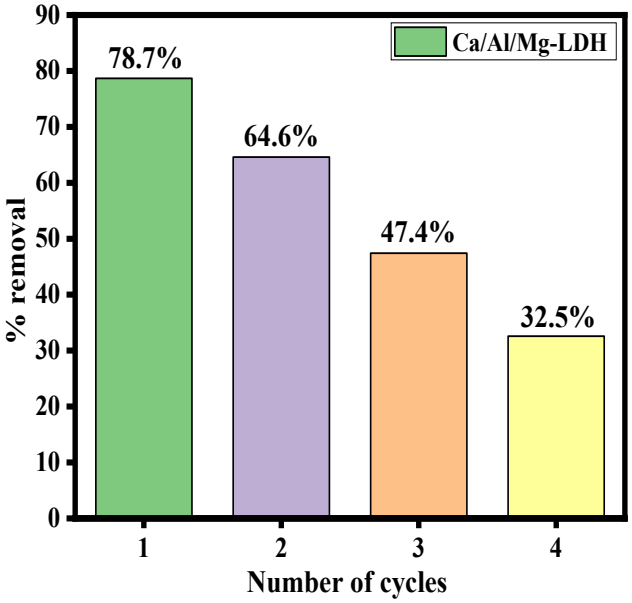

Figure 13. Reusability studies of Cu^{2+} adsorption onto the WsBio-LDH composite (Cu^{2+} conc. = 30 ppm, dose = 0.3 g, rpm = 220, pH = 6, time = 1 h).

3.7. *Comparison of Adsorbents*

A comparative evaluation of Cu^{2+} adsorption capacity of the WsBio-LDH composite with other reported adsorbents is presented in **Table 7**. The WsBio-LDH composite is compared with the other natural biochar for copper removal (Table 7), which showed good adsorption capacity for Cu^{2+} under optimal conditions, due to its functionalized surface, and displayed effective interaction with copper (II) ions in solution.

Table 7. Comparison of adsorption capacities of different adsorbents for removal of copper ions.

Adsorbent	Concentration range of Cu^{2+} (mg/L)	Contact time (min)	Sorbent dosage (g)	Adsorption capacity (mg/g)	References
WsBio-LDH composite	70	60	0.4	101.5	Present study
Magnetic biochar	50	360	1.0	65.55	(Kołodyńska and and Bąk 2018)
sawdust biochar	50	180	1.0	91.74	(Eleryan *et al.* 2024)
Biochar (solid waste)	100	180	0.1	5	(Hoslett *et al.* 2019)

Oxidized biochar (chitosan and PEI)	100	1400	4	26.7	(Liu *et al.* 2021)

4. Conclusion

This study highlights the potential of the WsBio-LDH composite as a cost-effective and efficient adsorbent for copper ion removal from aqueous solutions. LDH modification of WS biochar enhances its physicochemical characteristics and metal removal efficiency to 99.6% (adsorbent dose of 0.4 g and pH 6.0), which were optimized to 98.6%, respectively, using RSM. Isotherm studies showed that the WsBio-LDH composite followed the Langmuir model, suggesting an enhanced monolayer adsorption capacity. Kinetic analysis confirmed that the PSO model provided the best fit for the adsorbent, indicating that a monolayer adsorption occurred by chemisorption. Characterization of the WsBio-LDH composite using SEM, EDX, and FTIR confirmed its suitability for adsorption applications. SEM analysis revealed a highly porous surface morphology, while FTIR analysis identified key functional groups.

The study also examined the effects of contact time, adsorbent dose, pH, and metal ion concentration. Maximum removal efficiency of Cu^{2+} ions was observed at lower Cu^{2+} concentration, higher pH 6, and optimum adsorbent dose 0.4 g. RSM verified a good connection between statistical and experimental values with an error range of less than 1%. These findings suggest that the WsBio-LDH composite is an effective, cost-efficient, and sustainable adsorbent for the remediation of heavy metals from wastewater. Compared with previously reported biochar-based adsorbents, the WsBio-LDH composite demonstrates superior Cu^{2+} removal efficiency (>99.5%) under optimized conditions, outperforming wheat straw biochar and several metal-oxide-modified biochars reported in the literature. The enhanced performance is attributed to the synergistic effect of LDH incorporation, which increases surface charge density, active binding sites, and ion-exchange capacity.

A limitation of the present study is the gradual decline in adsorption efficiency during repeated regeneration cycles. The removal efficiency decreased from 78.7% to 32.5% after four cycles, indicating the need for improved regeneration methods and enhanced structural stability of the composite. Future studies should focus on optimizing regeneration protocols and evaluating long-term performance under continuous treatment conditions.

Despite the promising adsorption performance, certain limitations should be acknowledged. The adsorption experiments were conducted under batch conditions using synthetic wastewater, which may not fully represent complex industrial effluents comprising competing ions. Additionally, regeneration efficiency decreased after multiple cycles, indicating partial loss of active adsorption sites. These limitations highlight the need for further investigation under continuous-flow systems and real wastewater conditions.

4.1. *Future Scope and Practical Applications*

The proposed WsBio-LDH composite shows strong potential for real-time wastewater treatment applications due to its low-cost raw material, simple synthesis route, and high adsorption efficiency. Future research may focus on scaling up the process using fixed-bed or continuous-flow reactors, evaluating performance in real industrial effluents, and exploring adsorption of multi-metal systems. Additionally, integration of this adsorbent into hybrid treatment systems could enhance overall removal efficiency and sustainability.

Competing interests

The authors have no relevant financial or non-financial interests to disclose.

Funding

This research work was financially supported by the Vice Deanship of Research Chairs, King Saud University, Riyadh, KSA.

Data Availability Statement

The datasets generated and analyzed during the current study are available from the corresponding author upon reasonable request.

References

Abdipour H., and Hemati H. (2024). Sonocatalytic process of penicillin removal using - Fe_2O_3 / effect of different parameters / degradation mechanism/ kinetic study/optimisation with response surface model. *International Journal of Environmental Analytical Chemistry*, *104*(20), 8617–8638. https://doi.org/10.1080/03067319.2023.2207465

Adachi-Pagano M., Forano C., and Besse J.-P. (2003). Synthesis of Al-rich hydrotalcite-like compounds by using the urea hydrolysis reaction—control of size and morphology. *Journal of Materials Chemistry*, *13*(8), 1988–1993. https://doi.org/10.1039/B302747N

Afshar M., and Mofatteh S. (2024). Biochar for a sustainable future: Environmentally friendly production and diverse applications. *Results in Engineering*, *23*, 102433. https://doi.org/10.1016/j.rineng.2024.102433

Akhtar M., Sarfraz M., Ahmad M., Raza N., and Zhang L. (2025). Use of low-cost adsorbent for waste water treatment: Recent progress, new trend and future perspectives. *Desalination and Water Treatment*, *321*, 100914. https://doi.org/10.1016/j.dwt.2024.100914

Alprol A. E., Mansour A. T., Ibrahim M. E. E.-D., Ashour M., Alprol A. E., Mansour A. T., Ibrahim M. E. E.-D., and Ashour M. (2024). Artificial Intelligence Technologies Revolutionizing Wastewater Treatment: Current Trends and Future Prospective. *Water*, *16*(2), 314. https://doi.org/10.3390/w16020314

Al-Rashdi B. A. M., Johnson D. J., and Hilal N. (2013). Removal of heavy metal ions by nanofiltration. *Desalination*, *315*, 2–17. https://doi.org/10.1016/j.desal.2012.05.022

Bayantong A. R. B., Shih Y.-J., Ong D. C., Abarca R. R. M., Dong C.-D., and de Luna M. D. G. (2021). Adsorptive removal of dye in wastewater by metal ferrite-enabled graphene oxide nanocomposites. *Chemosphere*, *274*, 129518. https://doi.org/10.1016/j.chemosphere.2020.129518

Bej S., Swain S., Bishoyi A. K., Mandhata C. P., Sahoo C. R., and Padhy R. N. (2023). Wastewater-Associated Infections: A Public Health Concern. *Water, Air, & Soil Pollution*, *234*(7), 444. https://doi.org/10.1007/s11270-023-06431-4

Biswal B. K., and Balasubramanian R. (2023). Use of biochar as a low-cost adsorbent for removal of heavy metals from water and wastewater: A review. *Journal of Environmental Chemical Engineering*, *11*(5), 110986. https://doi.org/10.1016/j.jece.2023.110986

Cao X., Ma L., Gao B., and Harris W. (2009). Dairy-Manure Derived Biochar Effectively Sorbs Lead and Atrazine. *Environmental Science & Technology*, *43*(9), 3285–3291. https://doi.org/10.1021/es803092k

Chen R., Gan C., Cai B., Liu R., Xu W., Yin W., Li H., Yu L., and Yong Q. (2024). Co-adsorption and selective-adsorption of heavy metals and dyes from aqueous solution by bio-based humus/chitosan hydrogels. *Journal of Environmental Sciences*, *145*, 193–204. https://doi.org/10.1016/j.jes.2023.09.004

Cheung W. H., Szeto Y. S., and McKay G. (2007a). Intraparticle diffusion processes during acid dye adsorption onto chitosan. *Bioresource Technology*, *98*(15), 2897–2904. https://doi.org/10.1016/j.biortech.2006.09.045

Cheung W. H., Szeto Y. S., and McKay G. (2007b). Intraparticle diffusion processes during acid dye adsorption onto chitosan. *Bioresource Technology*, *98*(15), 2897–2904. https://doi.org/10.1016/j.biortech.2006.09.045

Das S., Singh C. K., Sodhi K. K., and Singh V. K. (2025). Circular economy approaches for water reuse and emerging contaminant mitigation: innovations in water treatment. *Environment, Development and Sustainability: A Multidisciplinary Approach to the Theory and Practice of Sustainable Development*, *27*(3), 5753–5794. https://doi.org/10.1007/s10668-023-04183-z

Dehghani M. H., Ahmadi S., Ghosh S., Othmani A., Osagie C., Meskini M., AlKafaas S. S., Malloum A., Khanday W. A., Jacob A. O., Gökkuş Ö., Oroke A., Martins Chineme O., Karri R. R., and Lima E. C. (2023). Recent advances on sustainable adsorbents for the remediation of noxious pollutants from water and wastewater: A critical review. *Arabian Journal of Chemistry*, *16*(12), 105303. https://doi.org/10.1016/j.arabjc.2023.105303

Elbagory M., EL-Khateeb N., El-Nahrawy S., El-Dein Omara A., Mohamed I., El-Sharkawy M., Zayed A., Goala M., Gupta D., Kumar P., Kumar P., and Širić I. (2025). Inclusion of key soil parameters in the modified contamination factor (MCF) model as a tool for assessing heavy metal pollution in agricultural soils. *Scientific Reports*, *15*(1), 42974. https://doi.org/10.1038/s41598-025-27110-w

Eleryan A., Aigbe U. O., Ukhurebor K. E., Onyancha R. B., Eldeeb T. M., El-Nemr M. A., Hassaan M. A., Ragab S., Osibote O. A., Kusuma H. S., Darmokoesoemo H., and El Nemr A. (2024). Copper(II) ion removal by chemically and physically modified sawdust biochar. *Biomass Conversion and Biorefinery*, *14*(8), 9283–9320. https://doi.org/10.1007/s13399-022-02918-y

El-Shafey S. E., Obada M. K., El-Shamy A. M., and Mohamed W. S. (2024). Silica/klucel nanocomposite as promising durable adsorbent for lead removal from industrial effluents. *Scientific Reports*, *14*(1), 26095. https://doi.org/10.1038/s41598-024-74680-2

Farooq, A., Li, X., Pan, G., Liu, Q., Wang, F., Chen, S., Zhao, G. and Hussain, F., (2025). Advancing green textile modification with deep eutectic solvents: from solvent design to industrial prospects. Journal of Molecular Liquids, 347(B), 128501. https://doi.org/ 10.1016/j.molliq.2025.128501.

Fouad, E.A., Ahmad, F. and Ahmed, N. (2017). Optimization of chromium extraction from aqueous solutions by emulsion liquid membrane. *Desalination and Water Treatment*, 65, 428-434. https://doi.org/10.5004/dwt.2017.20287 Frost R. L., and Kloprogge J. T. (1999). Infrared emission spectroscopic study of brucite. *Spectrochimica Acta Part A: Molecular and Biomolecular Spectroscopy*, *55*(11), 2195–2205. https://doi.org/10.1016/S1386-1425(99)00016-5

Gaetke L. M., Chow-Johnson H. S., and Chow C. K. (2014). Copper: toxicological relevance and mechanisms. *Archives of Toxicology*, *88*(11), 1929–1938. https://doi.org/10.1007/s00204-014-1355-y

Gräf T., Gummi K., Filser J., Thöming J., and Köser J. (2023). Improving Membrane Filtration for Copper Speciation: Optimal Salt Pretreatments of Polyethersulfone Membranes to Prevent Analyte Retention. *ACS Omega*, *8*(6), 5742–5751. https://doi.org/10.1021/acsomega.2c07355

Hagag M. A., El-Gayar D. A., Nosier S. A., and Mubarak A. A. (2017). Removal of heavy metals from industrial waste solutions by a rotating fixed bed of ion exchange resin. *Desalination and Water Treatment*, *100*, 178–184. https://doi.org/10.5004/dwt.2017.21794

Haleem N., Khattak A., Jamal Y., Sajid M., Shahzad Z., and Raza H. (2022). Development of poly vinyl alcohol (PVA) based biochar nanofibers for carbon dioxide (CO_2) adsorption. *Renewable and Sustainable Energy Reviews*, *157*, 112019. https://doi.org/10.1016/j.rser.2021.112019

Han F., Hessen A. S., Amari A., Elboughdiri N., and Zahmatkesh S. (2024). Heavy metal (Cu^{2+}) removal from wastewater by metal-organic framework composite adsorbent: Simulation-based- artificial neural network and response surface methodology. *Environmental Research*, *245*, 117972. https://doi.org/10.1016/j.envres.2023.117972

Hassan, A. M. M., Asif, M., Al-Mansur, M. A., Uddin, M. R., Alsufyani, S. J., Yasmin, F., & Khandaker, M. U. (2023). Characterization of municipal solid waste for effective utilization as an alternative source for clean energy production. *Journal of Radiation Research and Applied Sciences*, 16(4), 100683. https://doi.org/10.1016/j.jrras.2023.100683.

Hoslett J., Ghazal H., Ahmad D., and Jouhara H. (2019). Removal of copper ions from aqueous solution using low temperature biochar derived from the pyrolysis of municipal solid waste. *Science of The Total Environment*, *673*, 777–789. https://doi.org/10.1016/j.scitotenv.2019.04.085

Hussain, M. S., Ahmed, S., Irshad, M., Bibi, S. S., Asif, M., Sher, F., & Khan, M. K. (2024). Recent engineering strategies for enhancing C2+ product formation in copper-catalyzed CO2 electroreduction. Nano Materials Science, 8(1), 207-233. https://doi.org/10.1016/j.nanoms.2024.09.001.

Hussain N., Asif M., Shafaat S., Khan M. S., Riaz N., Iqbal M., Javed A., Butt T. A., Shaikh A. J., and Bilal M. (2025). Multilayer adsorption of reactive orange 16 dye onto Fe_2O_3/ZnO hybrid nanoadsorbent: mechanistic insights from kinetics, isotherms and dynamic light scattering studies. *Journal of Chemical Technology & Biotechnology*, *100*(1), 50–66. https://doi.org/10.1002/jctb.7753

Johnston A.-L., Lester E., Williams O., and Gomes R. L. (2021). Understanding Layered Double Hydroxide properties as sorbent materials for removing organic pollutants from environmental waters. *Journal of Environmental Chemical Engineering*, *9*(4), 105197. https://doi.org/10.1016/j.jece.2021.105197

Jafari A. J., Mansoorian H. J., Askarpour H., Salari M., Eslami F., Faraji M., Shomoossi F., Abdipour H., and Ansari F. J. (2025). Analyzing and optimizing the adsorption of metronidazole antibiotic on nano-scale pumice mine waste based RSM-CCD technique in water. *International Journal of Environmental Science and Technology*, *22*(6), 4091–4108. https://doi.org/10.1007/s13762-024-06102-9

Kabir E., Kim K.-H., and Kwon E. E. (2023). Biochar as a tool for the improvement of soil and environment. *Frontiers in Environmental Science*, *11*. https://doi.org/10.3389/fenvs.2023.1324533

Kameliya J., Verma A., Dutta P., Arora C., Vyas S., and Varma R. S. (2023). Layered Double Hydroxide Materials: A Review on Their Preparation, Characterization, and Applications. *Inorganics*, *11*(3), Article 3. https://doi.org/10.3390/inorganics11030121

Kołodyńska D., and and Bąk J. (2018). Use of three types of magnetic biochar in the removal of copper(II) ions from wastewaters. *Separation Science and Technology*, *53*(7), 1045–1057. https://doi.org/10.1080/01496395.2017.1345944

Kouniba S., Benbiyi A., Zourif A., and EL Guendouzi M. (2024). Optimization use of watermelon rind in the coagulation-flocculation process by Box Behnken design for copper, zinc, and turbidity removal. *Heliyon*, *10*(10), e30823. https://doi.org/10.1016/j.heliyon.2024.e30823

Kumar A., Schreiter I. J., Wefer-Roehl A., Tsechansky L., Schüth C., and Graber E. R. (2016). Chapter 5 - Production and Utilization of Biochar From Organic Wastes for Pollutant Control on Contaminated Sites. In M. N. V. Prasad & K. Shih (Eds.), *Environmental Materials and Waste* (pp. 91–116). Academic Press. https://doi.org/10.1016/B978-0-12-803837-6.00005-6

Liang, S., Feng, X., Li, X., Wang, Z., Miao, K., Feng, G. and Luo, X., 2026 Catalysis of nonstoichiometric Mn–Co spinel oxides in effective peroxymonosulfate activation: Structure–activity relationship and flow-through organic wastewater treatment. *Separation and Purification Technology*, 397(3), 138142. https://doi.org/10.1016/j.seppur.2026.138142.

Liu J., and Wang X. (2013a). Novel Silica-Based Hybrid Adsorbents: Lead(II) Adsorption Isotherms. *The Scientific World Journal*, *2013*(1), 897159. https://doi.org/10.1155/2013/897159

Liu J., and Wang X. (2013b). Novel Silica-Based Hybrid Adsorbents: Lead(II) Adsorption Isotherms. *The Scientific World Journal*, *2013*(1), 897159. https://doi.org/10.1155/2013/897159

Liu Q., Zang G.-L., and Zhao Q. (2021). Removal of copper ions by functionalized biochar based on a multicomponent Ugi reaction. *RSC Advances*, *11*(42), 25880–25891. https://doi.org/10.1039/D1RA04156H

Li, X., Li, Y., Li, Y., Zhang, M., & Zhu, J. (2026). Synthesis of Lignin-Derived Hierarchical Porous Carbon via Hydrothermal–Phosphoric Acid Synergistic Activation for Enhanced Adsorption of Tetracycline. Molecules, 31(3), 447, https://doi.org/10.3390/molecules31030447

Li, X., Ran, R., Zeng, W., Ren, S., Wang, Y., Zhu, A., & Zheng, C. (2025). Coffee shell as a green reductant for iron recovery from pyrite cinder: synergy of biomass-driven reduction and acid leaching. Minerals Engineering, 234, 109747, https://doi.org/10.1016/j.mineng.2025.109747.

Liu Y., Gao C., Liu L., Li Y., and Guo X. (2025). A photovoltaic powered ocean-based electrochemical system produces highly oxidizing active substances for simultaneous removal of antibiotics and heavy metals from mariculture wastewater. *Water Research*, *286*, 124177. https://doi.org/10.1016/j.watres.2025.124177

Luo Y., Gao B., Yue Q., and Li R. (2018). Application of enteromorpha polysaccharides as coagulant aid in the simultaneous removal of CuO nanoparticles and Cu^{2+}: Effect of humic acid concentration. *Chemosphere*, *204*, 492–500. https://doi.org/10.1016/j.chemosphere.2018.03.168

Lyu P., Li L., Huang J., Ye J., Zhu C., Xie J., Wang Z., Kang M., and Yan A. (2023). Enhancing sorption of layered double hydroxide-based magnetic biochar for arsenic and cadmium through optimized preparation protocols. *Bioresource Technology*, *388*, 129756. https://doi.org/10.1016/j.biortech.2023.129756

Ma Q., Qian Y., Su W., Shi L., Wang E., Yu A., Zheng J., and Lu Y. (2025). Degradation of agricultural polyethylene film by greater wax moth (*Galleria mellonell*a) larvae and screening of involved gut bacteria. *Ecotoxicology and Environmental Safety*, *303*, 118841. https://doi.org/10.1016/j.ecoenv.2025.118841

Mahmood, Z., Abbas, N., Naqvi, S.A.R., Gilani, M.R.H.S., Hussain, F., Ali, S.K., Iqbal, S., Mahmood, S., Abdelmohsen, S.A. and Alarfj, S.F. (2026). Visible-Light-Activated CuFe2O4/Zn-BTC Photocatalyst for Efficient Mineralization and Detoxification of Carbofuran in Industrial Effluents. Catalysis Letters, 156(6), 176. https://doi.org/10.1007/s10562-026-05418-0.

Mingming S., Hengze Z., Ye L., and Lingqi Z. (2023). The adsorption properties of steel slag-based porous geopolymer for Cu^{2+} removal. *Minerals Engineering*, *201*, 108225. https://doi.org/10.1016/j.mineng.2023.108225

Mokhtar M., Dickson S. E., Kim Y., and Mekky W. (2018). Preparation and characterization of ion selective membrane and its application for Cu^{2+} removal. *Journal of Industrial and Engineering Chemistry*, *60*, 475–484. https://doi.org/10.1016/j.jiec.2017.11.035

Mondal M. K. (2009). Removal of Pb(II) ions from aqueous solution using activated tea waste: Adsorption on a fixed-bed column. *Journal of Environmental Management*, *90*(11), 3266–3271. https://doi.org/10.1016/j.jenvman.2009.05.025

Nzediegwu C., Naeth M. A., and Chang S. X. (2021). Elemental composition of biochars is affected by methods used for its determination. *Journal of Analytical and Applied Pyrolysis*, *156*, 105174. https://doi.org/10.1016/j.jaap.2021.105174

Othman C. S., Salih Y. M., and Hamasalih L. O. (2023). Adsorption desulfurization of dibenzothiophene in a model and diesel fuel by hybrid activated charcoal/mixed metal oxide.

Petroleum Science and Technology, *41*(22), 2121–2140. https://doi.org/10.1080/10916466.2022.2108052

Patel M. R., and Panwar N. L. (2023). Biochar from agricultural crop residues: Environmental, production, and life cycle assessment overview. *Resources, Conservation & Recycling Advances*, *19*, 200173. https://doi.org/10.1016/j.rcradv.2023.200173

Priya K., Rani J., and Gwal S. (2025). Chapter 6 - Transforming agricultural residues to value-added products: waste to wealth. In S. Rai, A. K. Bhardwaj, & L. M. Colla (Eds.), *Sustainable Management of Agro-Food Waste* (pp. 69–85). Academic Press. https://doi.org/10.1016/B978-0-443-23679-2.00006-9

Qin, X., Cui, H., & Zhou, Q. (2023). Physisorption behaviors of organochlorine pesticides on the InP3 monolayer from theoretical insight. ACS omega, 8(35), 32168-32175, https://doi.org/10.1021/acsomega.3c04665.

Rashid R., Shafiq I., Akhter P., Iqbal M. J., and Hussain M. (2021). A state-of-the-art review on wastewater treatment techniques: the effectiveness of adsorption method. *Environmental Science and Pollution Research*, *28*(8), 9050–9066. https://doi.org/10.1007/s11356-021-12395-x

Riseh R. S., Vazvani M. G., Hassanisaadi M., and Thakur V. K. (2024). Agricultural wastes: A practical and potential source for the isolation and preparation of cellulose and application in agriculture and different industries. *Industrial Crops and Products*, *208*, 117904. https://doi.org/10.1016/j.indcrop.2023.117904

Rydz J., Šišková A., and Andicsová Eckstein A. (2019). Scanning Electron Microscopy and Atomic Force Microscopy: Topographic and Dynamical Surface Studies of Blends, Composites, and Hybrid Functional Materials for Sustainable Future. *Advances in Materials Science and Engineering*, *2019*(1), 6871785. https://doi.org/10.1155/2019/6871785

Olugbenga S. O., Adeleye P. G, Oladipupo S. B, Adeleye A. T, and John K. I. (2024). Biomass-derived biochar in wastewater treatment- a circular economy approach. *Waste Management Bulletin*, *1*(4), 1–14. https://doi.org/10.1016/j.wmb.2023.07.007

Shafiq M., Alazba A. A., and Amin M. T. (2025). Eco-friendly nanocomposite of manganese-iron and plant waste derived biochar for optimizing Pb^{2+} adsorption: A response surface methodology approach. *Desalination and Water Treatment*, *322*, 101091. https://doi.org/10.1016/j.dwt.2025.101091

Shiriazar M. A., Sepehr E., Maleki R., Khodaverdiloo H., Asadzadeh F., Dovlati B., and Rengel Z. (2022). Arsenate removal from aqueous solutions by Mg/Fe-LDH-modified biochar derived from apple tree residues. *Earth and Environmental Science Transactions of The Royal Society of Edinburgh*, *113*(2), 149–158. https://doi.org/10.1017/S1755691022000019

Shoudho K. N., Khan T. H., Ara U. R., Khan M. R., Shawon Z. B. Z., and Hoque M. E. (2024). Biochar in global carbon cycle: Towards sustainable development goals. *Current Research in Green and Sustainable Chemistry*, *8*, 100409. https://doi.org/10.1016/j.crgsc.2024.100409

Sun X., Li S., Xiong Y., and You Y. (2022). Flocculation performance and evaluation of a sulfur-containing tannin flocculant for Cu^{2+} removal. *Separation and Purification Technology*, *303*, 122277. https://doi.org/10.1016/j.seppur.2022.122277

Syed, N.H., Haq, I., Ahmad, F., Khan, N.A., Habib, M., Ahmad, N. and Rind, I.K., (2024). A Low Cost Wastewater Reclamation Unit comprising a Lamella Settler for reducing Fresh Water Usage in Carwash Stations. *Engineering, Technology & Applied Science Research*, 14(5), 16221-16228. https://doi.org/10.48084/etasr.8066.

Tabassam M. N., Haseeb M., Habib M. A. B., Murtaza R., Ali S., Malik M. R., Numan M., Mahmood M., Mustafa Z., and Khan W. Z. (2025). Next-Generation Adsorbents for Wastewater Remediation: A Nanotechnology-Driven and AI-Enabled Breakthrough Towards Clean Water. *Scholars Journal of Physics, Mathematics and Statistics*, *12*(08), 323–345. https://doi.org/10.36347/sjpms.2025.v12i08.001

Tanweer, A., Taqvi, S. A. A., Kazmi, B., Khatoon, S., Taha, M., Nadir, M., . . . Ahmad, N. (2025). Advancing algae-based Bioenergy: Techno-Economic assessment of hydrogen and biochar production from algal biomass. Biomass and Bioenergy, 200, 108039, https://doi.org/10.1016/j.biombioe.2025.108039

Torabideh M., Khalooei M., Rajabizadeh A., Abdipour H., and Zeinali S. (2025). Optimisation of mercury adsorption by ZIF-8 from aqueous solutions through response surface methodology. *International Journal of Environmental Analytical Chemistry*, *105*(18), 6910–6932. https://doi.org/10.1080/03067319.2024.2432583

Trinh H. B., Lee J., Kim S., Lee J., Aceituno J. C. F., and Oh S. (2021). Selective Recovery of Copper from Industrial Sludge by Integrated Sulfuric Leaching and Electrodeposition. *Metals*, *11*(1), Article 1. https://doi.org/10.3390/met11010022

Wang, D., Hu, W., Zheng, Y., Cheng, H., Lu, X., He, Z., Giannakis, S., Song, S. and Ma, J., (2026). Mechanistic insights into hexamethylphosphoramide degradation and phosphorus recovery via mZVI/O3: Beyond conventional oxidation through iron-phosphorus speciation. *Chemical Engineering Journal*, 538, 176658. https://doi.org/10.1016/j.cej.2026.176658.

Wang L., Shi C., Wang L., Pan L., Zhang X., and Zou J.-J. (2020). Rational design, synthesis, adsorption principles and applications of metal oxide adsorbents: a review. *Nanoscale*, *12*(8), 4790–4815. https://doi.org/10.1039/C9NR09274A

Wang T., Liu W., Xiong L., Xu N., and Ni J. (2013). Influence of pH, ionic strength and humic acid on competitive adsorption of Pb(II), Cd(II) and Cr(III) onto titanate nanotubes. *Chemical Engineering Journal*, *215–216*, 366–374. https://doi.org/10.1016/j.cej.2012.11.029

Wang Y., Zheng K., Jiao Z., Zhan W., Ge S., Ning S., Fang S., and Ruan X. (2022). Simultaneous Removal of Cu^{2+}, Cd^{2+} and Pb^{2+} by Modified Wheat Straw Biochar from Aqueous Solution: Preparation, Characterization and Adsorption Mechanism. *Toxics*, *10*(6), Article 6. https://doi.org/10.3390/toxics10060316

Xu S., Zhang L., Zhao J., Cheng J., Yu Q., Zhang S., Zhao J., and Qiu X. (2020). Remediation of chromium-contaminated soil using delaminated layered double hydroxides with different divalent metals. *Chemosphere*, *254*, 126879. https://doi.org/10.1016/j.chemosphere.2020.126879

Yan F., Chen H., Chi T., Lu J., Shen X., Xie F., Wang P., and Zhang Z. (2025). Highly efficient and regenerable amine-impregnated adsorbents: Mechanistic insights into glycerol modification for enhanced direct air capture. *Chemical Engineering Journal*, *520*, 166450. https://doi.org/10.1016/j.cej.2025.166450

Yrjälä K., and Zheng H. (2021). Renewable Energy from Woody Biomass of Poplar and Willow SRC Coupled to Biochar Production. In P. Pathak & R. Ranjan Srivastava (Eds.),

Alternative Energy Resources (pp. 133–150). Springer. https://doi.org/10.1007/698_2020_647

Zakaria K. K., Farag H. A., and El-Gayar D. A. (2023). Removal of Cu^{2+}, Fe^{2+} and SO_4^{2-} ions from industrial wastewater by ion exchange resins contained in a rotating perforated cylindrical basket of different heights. *Scientific Reports*, *13*(1), 3248. https://doi.org/10.1038/s41598-023-29956-4

Zhang D., Wu B., Wang T., Yılmaz M., Sharma G., Kumar A., and Shi H. (2025). Multi-mechanism synergistic adsorption of lead and cadmium in water by structure-functionally adapted modified biochar: A review. *Desalination and Water Treatment*, *322*, 101156. https://doi.org/10.1016/j.dwt.2025.101156

Zhang Y., Luo C., Wang H., Han L., Wang C., Jie X., and Chen Y. (2016). Modified adsorbent hydroxypropyl cellulose xanthate for removal of Cu^{2+} and Ni^{2+} from aqueous solution. *Desalination and Water Treatment*, *57*(56), 27419–27431. https://doi.org/10.1080/19443994.2016.1177733

Zou Y., Liu Y., Wang X., Sheng G., Wang S., Ai Y., Ji Y., Liu Y., Hayat T., and Wang X. (2017). Glycerol-Modified Binary Layered Double Hydroxide Nanocomposites for Uranium Immobilization via Extended X-ray Absorption Fine Structure Technique and Density Functional Theory Calculation. *ACS Sustainable Chemistry & Engineering*, *5*(4), 3583–3595. https://doi.org/10.1021/acssuschemeng.7b00439